Cloud Formation on Exoplanets: Different Cloud Regimes for Changing Global Parameters

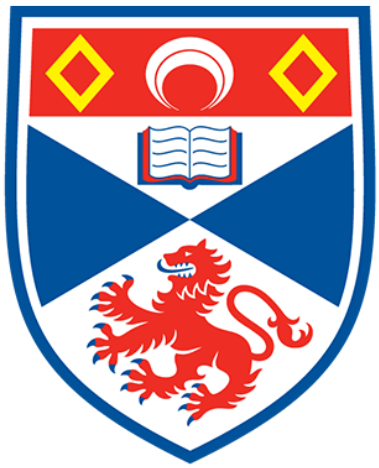

University of St Andrews

Robb Calder

E-mail: rc241@st-andrews.ac.uk

Supervisor: Prof Christiane Helling

August 2021

Contents

1 Introduction **1**

2 Background **2**
2.1 Hot Jupiters 2
2.2 Model Grid 2
2.3 Global Circulation Models 3

3 Methodology **3**
3.1 Extracting 1D Profiles 3
3.2 Modelling Approach 4

4 Results **4**
4.1 Total Nucleation Rate 5
4.2 Mean Molecular Weight 10
4.3 Mean Grain Size and Ionisation Rate 10

5 Discussion **11**
5.1 Equatorial Superrotation 11
5.2 Model Limitations 12

6 Conclusions **12**

7 Acknowledgments **12**

1 Introduction

The study of exoplanet atmospheres is essential for finding life in our universe. The ability to determine the chemical makeup of an atmosphere allows us to search them for certain species (elements and compounds), some of which could be indicators of biological activity (bio-tracers). Due to the vast distances between our solar system and these planets, and the fact that most of these atmospheres block light from the surface, we can only observe exoplanet atmospheres. Therefore, bio-tracers remain the only method for finding life in our universe.

We observe exoplanet atmospheres using a technique known as the transit method. This procedure involves monitoring a star for a regular drop in its brightness caused by a planet passing in front of the star during its orbit. This 'transit' is typically observed using multiple wavelengths to see how the atmosphere interacts with different types of light. The different species in the atmosphere will absorb different wavelengths of light, leading to a different light curve (brightness as a function of time) for each wavelength.

Any models used to explain transit observations of exoplanet atmospheres need to account for cloud formation. The cloud layers block stellar light passing through the atmosphere, limiting the depth to which the atmosphere is observable. Also, the species that are used to form solid clouds become depleted from the gas phase, and given that we cannot see into the clouds, this makes these species appear less abundant than they actually are.

Detailed cloud formation models have been produced for the planets HAT-P-7b [9] and WASP-43b [10]. Further work includes a comparison study of cloud formation for a host of exoplanets [11]. However, it is still not understood how cloud formation is affected by changing global parameters such as planetary effective temperature and host star type. Understanding how these parameters affect cloud formation will allow us to predict the cloud properties of upcoming observation targets, and thus allow us to better explain these observations.

This work uses a grid of 3D GCMs (global circulation models) of Hot Jupiter exoplanets as input for cloud formation simulations (see section 2.1 for a definition of Hot Jupiters). Several 1D temperature-pressure profiles were extracted from each GCM and used as input for the simulations. The cloud properties for each model are compared to identify trends in cloud formation across the model grid. **Note: the results shown here form part of a larger collaborative project undertaken within the Centre for Exoplanet Science. The results of the full project will be shown in an upcoming paper by Helling et al**.

2 Background

2.1 Hot Jupiters

Due to the limited resolution of even the most modern telescopes as well as limited observation times, observations of atmospheres inherently favour larger planets with shorter orbital periods, known as Hot Jupiters. The detailed study of such planets will give insight into complex atmospheric processes that also apply to smaller, earth-like exoplanets.

The proximity of Hot Jupiters to their host star ensures that they are tidally locked, i.e., their rotational period is the same as their orbital period. This means that, unlike Earth, one side of the planet is always facing the star and one side is always facing away from the star. We say that the planets have a permanent day-side and a permanent night-side.

The four key points on tidally-locked exoplanets, defined by their longitude (ϕ) and latitude (θ) co-ordinates, are the sub-stellar point (the point facing directly towards the star with $(\phi, \theta) = (0°, 0°)$), the evening terminator, with $(\phi, \theta) = (90°, 0°)$, the morning terminator, with $(\phi, \theta) = (270°, 0°)$) and the anti-stellar point (the point facing directly away from the star with $(\phi, \theta) = (180°, 0°)$).

2.2 Model Grid

This work investigates how cloud formation is affected by two global parameters: planetary effective temperature and host stellar type.

The effective temperature is a combination of the planetary equilibrium temperature T_{eq} and the internal temperature T_{int} (T_{int} is taken as 200K for the entire grid [2]).

$$T_{eff}^4 = T_{int}^4 + T_{eq}^4 \tag{1}$$

$$T_{eq}^4 = \frac{f L_*}{16 \pi \sigma a^2} \tag{2}$$

where f is the heat re-distribution factor (taken as 2 when the stellar radiation falls on the day-side only), L_* is the luminosity of the host star, σ is the Stefan-Boltzmann constant and a is the semi-major axis of the planet (the orbital distance in the case of Hot Jupiters). The grid used here (produced by Baeyens et al. [2]) samples 12 effective temperatures in increments of 200K between 400K and 2600K.

Stars are classified using seven types based upon their effective temperature: O,B,A,F,G,K and M, with O stars being the hottest stars and M stars being the coolest (the number after

the stellar class further categorises the luminosity within the class). Bayens et al. use 4 stellar types: F5 (T_{star}=6500K), G5 (T_{star}=5650K), K5 (T_{star}=4250K) and M5 (T_{star}=3100K).

If two planets have the same effective temperature, but one orbits a hot star and one orbits a cold star (relatively speaking), then the planet orbiting the cold star must orbit closer to that star to preserve the same effective temperature. This means that the planet will have a shorter orbital period, and given that the planets are tidally locked, they will also have a shorter rotational period. This implies that the planet rotates faster, which increases the Coriolis force that it experiences. Given that the Coriolis force opposes the horizontal mixing in the atmosphere, a faster rotation rate means that there is less efficient re-distribution of heat between the day and the night side. Therefore, planets orbiting cooler host stars will have a greater day-night side temperature contrast.

2.3 Global Circulation Models

The cloud formation code uses a grid (grid here refers to a set of models with different values for the global parameters) of GCMs produced by Baeyens et al. as input [2]. Global circulation models are simulations of exoplanet atmospheres that account for heat transfer via the host star as well as horizontal and vertical mixing of the gas in the atmosphere due to global weather patterns.

The GCMs are spherical data-cubes with 3 positional co-ordinates: latitude, longitude and pressure (pressure is used here as a substitute for atmospheric height, with increasing pressure in deeper parts of the atmosphere). Each co-ordinate contains the temperature of the gas phase and the velocity vector (v_x,v_y and v_z). All models used in this work have a surface gravity of 10ms^{-2} and a radius of 1.35 Jupiter radii.

There is a caveat to bear in mind with regards to the GCMs. The material abundances (relative abundances of each element) are consistent across all the models (this is also the case for the cloud formation simulations). However, these properties vary across different host star types and will thus vary for the planets that form from the by-products of star formation. Therefore, this work does not account for varying elemental abundances for planets that form around different host stars.

3 Methodology

3.1 Extracting 1D Profiles

The cloud formation model used 48 pressure-temperature profiles from each GCM, extracted at equidistant longitudes across the equatorial plane ($\theta = 0°$). The longitudes sampled ranged from ϕ =0° to ϕ =345° in 15° intervals. These profiles were then used as

input for a kinetic cloud formation model coupled with a chemical network.

3.2 Modelling Approach

Cloud formation occurs via several stages (see Helling et al. [8] for a visual representation of this process). Firstly, molecular clusters known as nucleation seeds form from the gas phase. For a monomer (molecules that combine to form molecular clusters) to form nucleation seeds effectively, it must be thermally stable (i.e., it must not break down due to high temperatures) and it must be available in a gaseous state. This work considers 4 nucleation species: TiO_2, SiO, KCl and NaCl.

Other materials then accrete onto these seeds via surface chemical reactions to form the cloud particles. Materials will only accrete onto the seeds if they are also thermally stable, implying that cloud formation is heavily dependant on the thermodynamic conditions (temperature and pressure) of the local gas phase. The nucleation species will themselves also participate in bulk growth, meaning that there is competition for the elements involved. A total of 16 bulk materials participate in bulk growth for this work: TiO_2, Mg_2SiO_4, $MgSiO_3$, MgO, SiO, SiO_2, Fe, FeO, FeS, Fe_2O_3, $FeSiO_4$, Al_2O_3, $CaTiO_3$, $CaSiO_3$, NaCl and KCl. They form via 132 surface reactions.

If the drag force due to the moving atmosphere is strong enough, the cloud particles couple with the gas phase and move with wind currents. As the cloud particles grow, they decouple from the wind currents and begin to fall through the atmosphere due to gravity.

The changing thermodynamic conditions mean that some of the accreted materials are no longer thermally stable, therefore they evaporate from the particles. The cloud particles continue to fall until the rising temperatures cause them to evaporate entirely. The accumulation of material due to bulk growth depletes the local gas phase of materials, while the evaporation of the materials from the cloud particles enriches the gas phase.

The approach for modelling these processes is the same as that used in Helling et al. [10], and a detailed discussion of the numerical details can be found in section 2.4 of Helling and Woitke [17].

4 Results

Cloud formation properties are shown in this work for a selection of the models in the grid. For a discussion of the results for the entire grid, refer to the upcoming paper by Helling et al.

This work considers 3 of the effective temperatures in the grid: 800K, 1600K and 2400K.

An effective temperature of 2400K describes Ultra-Hot Jupiters such as WASP-103b [5], WASP-121b [4] and HAT-P-7b [16], while an effective temperature of 1600K describes Hot Jupiters, such as WASP-43b [7] and HD209458b [15]. While not as common, an effective temperature of 800K describes 'Warm Saturns' such as HAT-P-6b [6].

To determine the various cloud regimes for each model, this work examines 3 properties related to cloud formation: nucleation rate, mean molecular weight and atmospheric ionisation rate. Figures 1, 2, 3 and 4 show these three properties (in addition to the extracted pressure-temperature profiles) for each of the 4 stellar types, for each of the 3 effective temperatures described above. The fourth row of each figure has the surface averaged mean grain size overlayed with a contour line showing the ionisation rate threshold for an ionosphere (see section 4.3). The grey mask shows the regions where cloud formation does not take place.

4.1 Total Nucleation Rate

The nucleation rate is the rate at which nucleation seeds form spontaneously from the gas phase (measured in [$cm^{-3}s^{-1}$]). It is used to identify the various cloud regimes (where the clouds form) throughout the planetary atmosphere. The total nucleation rate is the sum of the nucleation rate for each of the 4 nucleation species considered in this work.

For the T_{eff}=800K models, the nucleation rate on the night side is fairly high (between 10^{-1} and 10^{3} [$cm^{-3}s^{-1}$]) below 10^{-1} bar across all stellar types (1 bar is roughly equivalent to the surface pressure on earth). Above 10^{-1} bar, there is a gradual decrease in the nucleation rate (due to the gas temperature increasing) down to around 10^{-9} [$cm^{-3}s^{-1}$] at 10 bar. Above 10 bar, the nucleation ceases as the temperatures become too high for cloud formation. On the day side, the nucleation rate is lower (between 10^{-5} and 10^{-3} [$cm^{-3}s^{-1}$]), but non-negligible. There is also a thin layer (located at 10^{-2} bar) of increased nucleation extending onto the day-side from the morning terminator up to the sub-stellar point. This effect is present for all stellar types, but is less extended for the F star model.

For the T_{eff}=1600K models, the nucleation rate is lower across the night side than for the T_{eff}=800K models (between 10^{-5} and 10^{-1} [$cm^{-3}s^{-1}$]) for all stellar types. Only patches of the atmosphere below 10^{-2} bar exceed 10^{-1} [$cm^{-3}s^{-1}$]. Nucleation on the day-side is limited to the thin layer emerging from the morning terminator that also exists for the T_{eff}=800K models. This layer is narrower for the K and the M star models, and extends across the day-side completely for the M star model.

For the T_{eff}=2400K models, there is nucleation on the night-side only below 1 bar. The nucleation rate in this region is high (between 10^{-1} and 10^{3} [$cm^{-3}s^{-1}$]), but is slightly lower for the M star model. The nucleation rate is also higher near the morning terminator than near the evening terminator for night-side of these models. Nucleation is virtually non-existent on the day-side for all stellar types. There is limited nucleation near the evening

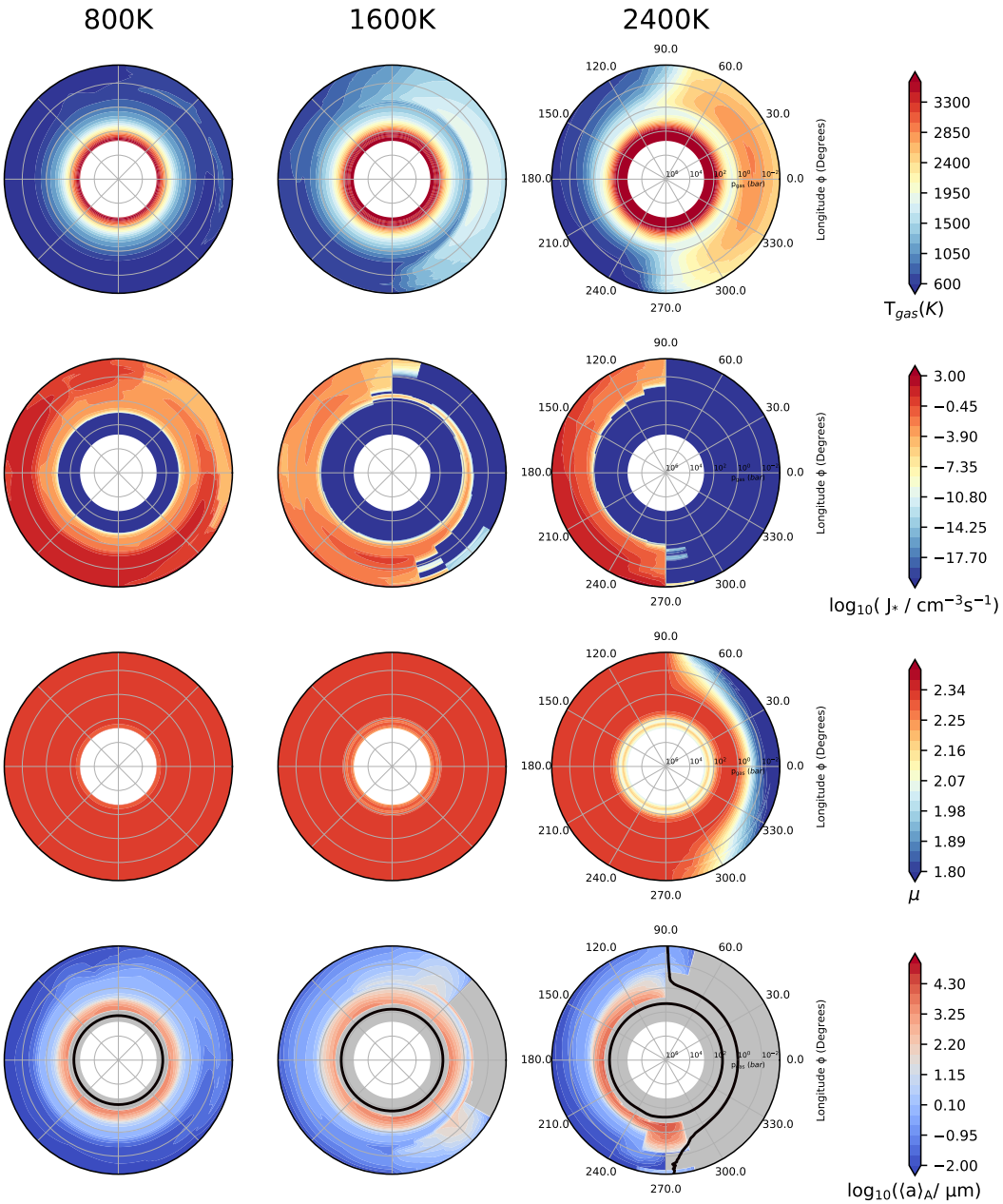

Figure 1: 2D equatorial plane slices ($\theta = 0$) for the 1D profiles extracted from the 3D GCMs showing the main cloud formation properties. The cloud formation properties are as follows: local gas temperature [K] (first row), total nucleation rate [$\log_{10}(\ J_*\ /\ \mathrm{cm}^{-3}\mathrm{s}^{-1})$] (second row), mean molecular weight (third row) and surface averaged mean particle size [$\log_{10}(\langle \mathrm{a} \rangle_\mathrm{A} / \ \mu\mathrm{m})$] overlayed with the ionisation rate threshold for an ionosphere (fourth row). These properties are shown for 3 planetary effective temperatures: 800K, 1600K and 2400K. All models have g=10ms^{-2} and orbit M stars. The outer limit for the pressure is fixed at $10^{3.5}$ bar for all models.

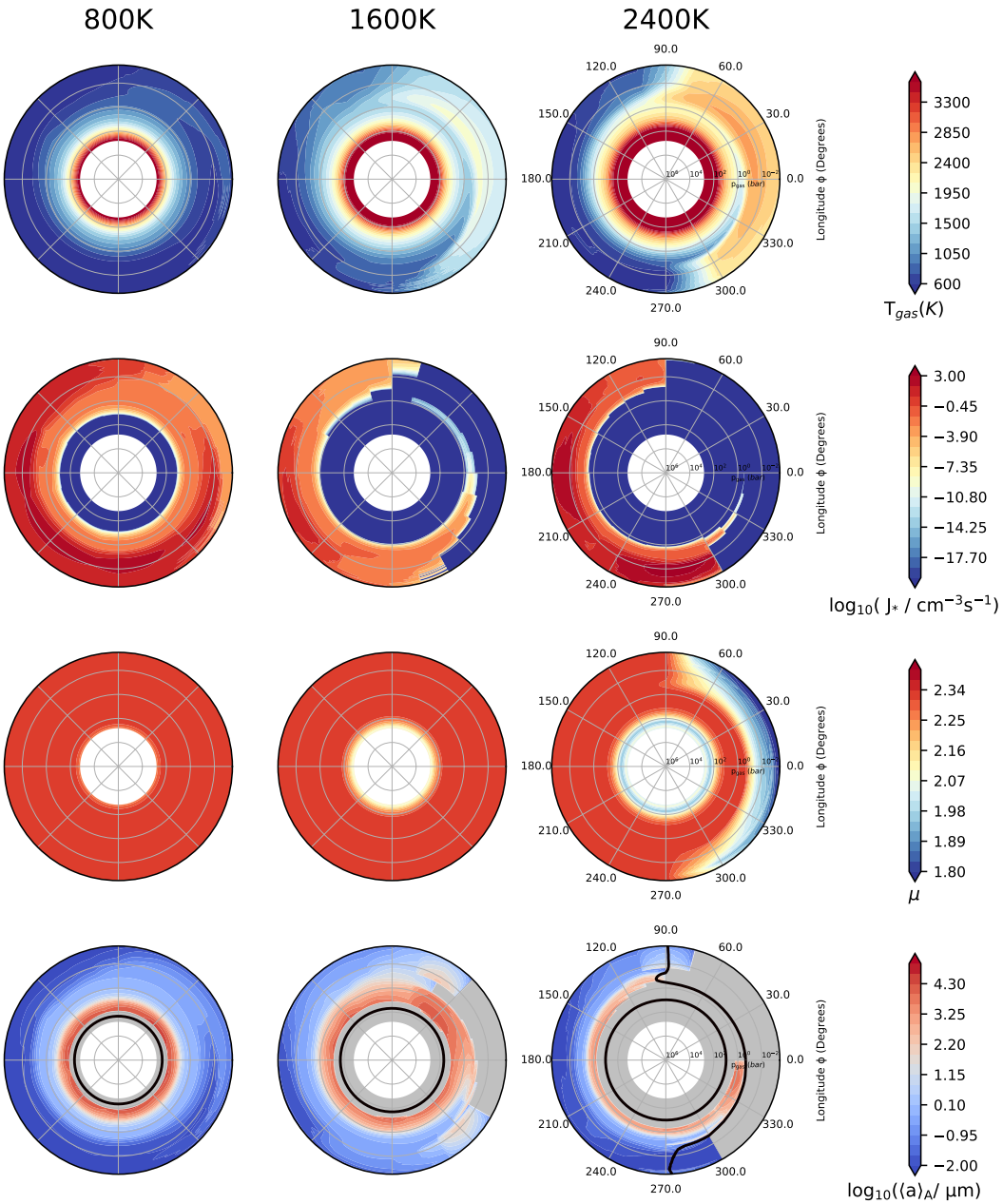

Figure 2: 2D equatorial plane slices ($\theta = 0$) for the 1D profiles extracted from the 3D GCMs showing the main cloud formation properties. The cloud formation properties are as follows: local gas temperature [K] (first row), total nucleation rate [$\log_{10}$(J_* / $cm^{-3}s^{-1}$)] (second row), mean molecular weight (third row) and surface averaged mean particle size [$\log_{10}$ ($\langle a \rangle_A$/ μm)] overlayed with the ionisation rate threshold for an ionosphere (fourth row). These properties are shown for 3 planetary effective temperatures: 800K, 1600K and 2400K. All models have g=10ms^{-2} and orbit K stars. The outer limit for the pressure is fixed at $10^{3.5}$ bar for all models.

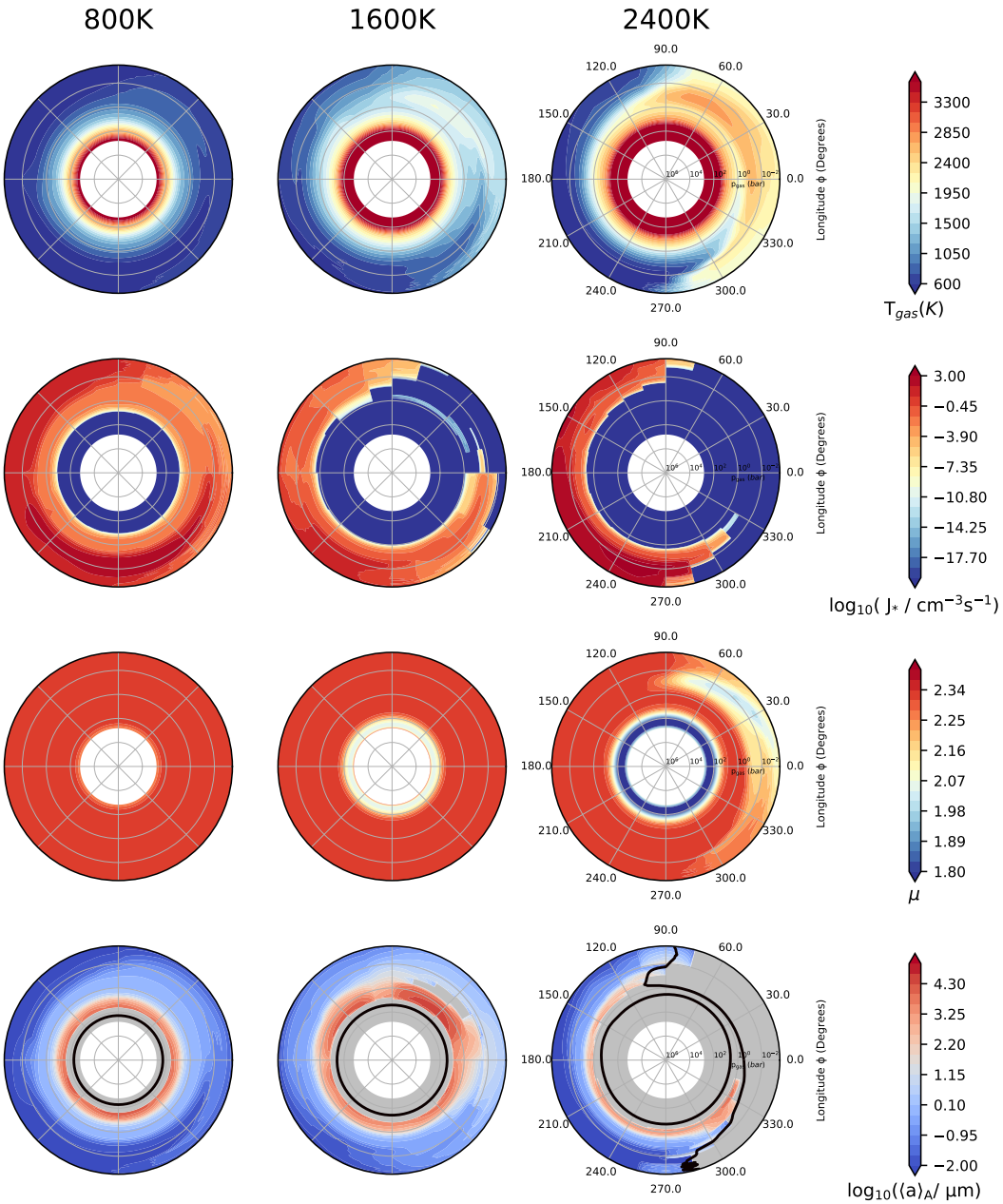

Figure 3: 2D equatorial plane slices ($\theta = 0$) for the 1D profiles extracted from the 3D GCMs showing the main cloud formation properties. The cloud formation properties are as follows: local gas temperature [K] (first row), total nucleation rate [$\log_{10}$(J_* / $cm^{-3}s^{-1}$)] (second row), mean molecular weight (third row) and surface averaged mean particle size [$\log_{10}$ ($\langle a \rangle_A$/ μm)] overlayed with the ionisation rate threshold for an ionosphere (fourth row). These properties are shown for 3 planetary effective temperatures: 800K, 1600K and 2400K. All models have g=10ms^{-2} and orbit G stars. The outer limit for the pressure is fixed at $10^{3.5}$ bar for all models.

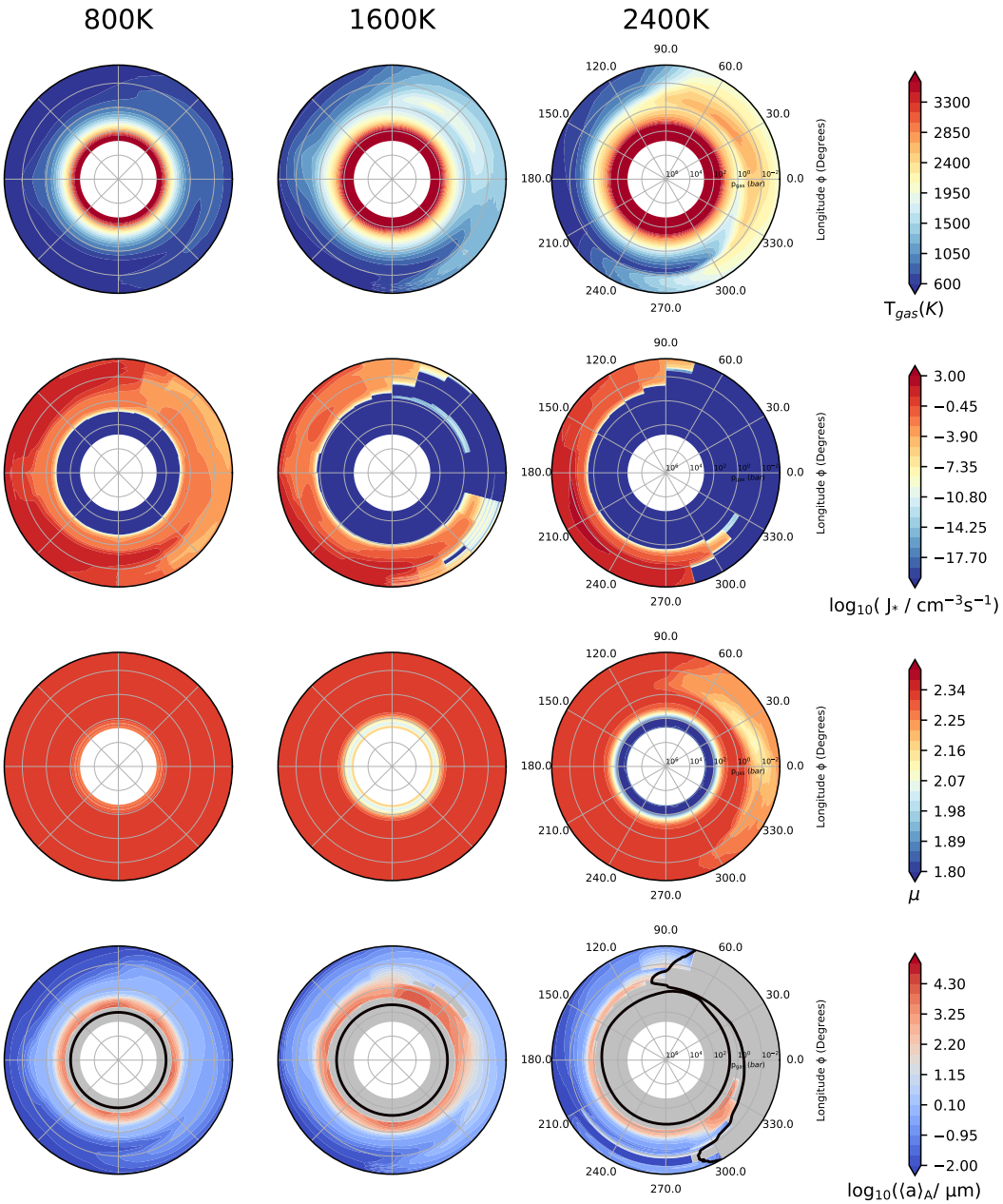

Figure 4: 2D equatorial plane slices ($\theta = 0$) for the 1D profiles extracted from the 3D GCMs showing the main cloud formation properties. The cloud formation properties are as follows: local gas temperature [K] (first row), total nucleation rate [$\log_{10}(\ J_* \ / \ cm^{-3}s^{-1})$] (second row), mean molecular weight (third row) and surface averaged mean particle size [$\log_{10}(\langle a \rangle_A / \ \mu m)$] overlayed with the ionisation rate threshold for an ionosphere (fourth row). These properties are shown for 3 planetary effective temperatures: 800K, 1600K and 2400K. All models have g=10ms^{-2} and orbit F stars. The outer limit for the pressure is fixed at $10^{3.5}$ bar for all models.

terminator on the day-side for the G, F and K star models, but not for the M star model.

4.2 Mean Molecular Weight

The mean molecular weight is defined as the mean mass of a particle in the atmosphere (given in atomic mass units). This property can be used to calculate the scale height of the atmosphere:

$$H = \frac{k_B T_{gas}}{\mu g_P} \tag{3}$$

where k_B is the Boltzman constant, T_{gas} is the local gas temperature, μ is the mean molecular weight and g_P is the planet's surface gravity. This is then used to determine size of the planetary atmosphere as the planet completes a transit of the host star, making the mean molecular weight an essential property for interpreting transit measurements [1]. Most GCMs assume a constant mean molecular weight of 2.35 (the value expected for a molecular hydrogen dominated atmosphere) throughout the atmosphere, however previous work has shown this not to be the case for Hot Jupiters [11].

Both the T_{eff}=800K and the T_{eff}=1600K models for all stellar types have a mean molecular weight of 2.35 throughout their atmosphere below 100 bar. Therefore, the assumption of a constant mean molecular weight for these atmospheres is valid.

For the T_{eff}=2400K models this not the case. On the day-side of the F star model, the mean molecular weight ranges from 2.10 to 2.25, and on the day-side of the G star model, the mean molecular weight ranges from 2.00 to 2.25. For both of these models, the lowest mean molecular weight occurs at a 'cold spot' at 10^{-2} bar. This region is more extended for the G star model (between ϕ=15° and ϕ=90°) than for the F star model (between ϕ=0° and ϕ=45°).

The day-side mean molecular weight for the M and the K star models at T_{eff}=2400K is much lower, dropping below 1.8 across the atmosphere. It is also more uniform across the day-side and it decreases consistently with pressure (i.e., there are no localised 'cold spots'). The mean molecular weight drops below 1.8 below 10^{-2} bar for the M star, whereas it only drops below 1.8 at the very edge of the pressure axis (below 10^{-3} bar) for the K star model.

4.3 Mean Grain Size and Ionisation Rate

The high day-side temperatures on Hot Jupiters can result in the gas phase becoming thermally ionised. Models of HAT-P-7b show an ionosphere that reaches the deeper layers of the atmosphere on the day-side [13]. If the ionosphere overlaps with the cloud layers on the

day-side, then this can alter the chemistry within the clouds and potentially even introduce lightning processes [12].

The degree of ionisation is measured as the ratio of the free electron pressure and the total pressure

$$f_e = \frac{p_e}{p_e + p_g} \tag{4}$$

where p_e is the free electron pressure and p_g is the gas pressure. A minimum value of f_e=10^{-7} is proposed as the threshold for an ionosphere [13]. The size of the cloud particles (measured here as the surface averaged mean grain size) must also be large enough for the particles to hold charge (the exact size threshold is undetermined).

The T_{eff}=800K and T_{eff}=1600K models for all stellar types have a sufficiently high ionisation rate only in the inner layers of the atmosphere, above 100 bar. There is no cloud formation above 100 bar for any of these models, therefore it is unlikely that these planets will have ionised cloud layers.

For the models where T_{eff}=2400K, the ionosphere for the M star model has limited overlap with the cloud formation at the terminator regions, but the grain sizes are small (below $10^{1.5}\mu$m). For the other stellar types, the thin layer of cloud formation on the day-side reaches the edge of the ionosphere (more so for the K star model). This indicates that there is the potential for the outer cloud layers to become ionised for these planetary models.

5 Discussion

5.1 Equatorial Superrotation

The cloud formation on the day-side of all the T_{eff}=1600K and T_{eff}=2400K models is driven primarily by prograde equatorial super-rotation (super-sonic winds in the same direction as the planet's rotation). Equatorial super-rotation is a common outcome for Hot Jupiter GCMs [3],[14] and is discussed for this grid in Baeyens et al. [2]. They note that only the faster rotating models (for this work, the M star model model with T_{eff}=2400K) do not show a prograde equatorial flow.

The super-rotation drives colder air onto the day-side, resulting in a 'jet' of cool gas protruding from the morning terminator. Cloud formation on the day-side is therefore limited to the jet. This feature is more prominent for the T_{eff}=1600K models and the slower rotators (F and G star models).

5.2 Model Limitations

The ionisation rate discussed here is only valid for thermal ionisation, i.e., ionisation due to extreme temperatures. This model does not account for ionisation due to cosmic rays or stellar irradiation, which could potentially extend the ionosphere deeper into the atmosphere. This effect would depend on whether or not the atmosphere is opaque to such radiation (i.e., whether or not the radiation can penetrate the atmosphere) in the day-side cloud layers. A discussion of opacity for these models will be included in future work by Helling et al.

6 Conclusions

A grid of global circulation models was used as input for a kinetic cloud formation model couped with a chemical network. This was done to study how cloud formation on Hot Jupiters is affected by varying the planetary effective temperature and the host star type. The following trends were identified:

- The colder Hot Jupiters (T_{eff}=800K) experience cloud formation on the day and night sides, with less cloud formation on the day-side. Hot Jupiters with T_{eff}=1600K, experience limited cloud formation on the day-side in a thin layer near the evening terminator caused by equatorial superrotation, which is more extended for F and G stars. Ultra-Hot Jupiters (T_{eff}=2400K) experience very limited day-side cloud formation near the evening terminator, and none at all for the M star models.
- Only the Ultra-Hot Jupiters have a mean molecular weight that varies throughout the atmosphere. There exists a 'cool spot' ($\mu \approx 2$) of lower mean molecular weight on the day-side of the F and the G star models, and $\mu < 1.8$ in the outer pressure layers for the K and the M stars.
- Only Ultra-Hot Jupiters have an ionosphere that overlaps with the cloud layers on the day-side. However, photo-ionisation will need to be incorporated into the modelling process to explore a potentially deeper ionosphere.

Given that cloud formation on the day-side of Hot and Ultra-Hot Jupiters is made possible by the transfer of cool air onto the day-side by equatorial super-rotation, a detailed understanding of this phenomenon is key for the improvement of cloud formation models. Since the day-sides of the Ultra-Hot Jupiter models have a non-constant mean molecular weight, future GCMs of such planets should use a dynamic mean molecular weight. Also, the day-side cloud layers on Ultra-Hot Jupiters will experience thermal ionisation, and the implications of this (lightning processes etc.) will require further study.

7 Acknowledgments

I would like to the thank my supervisor Professor Christiane Helling, for taking me on as a summer researcher, helping guide my research aims and assisting me during the difficult

aspects of this project. I would also like to thank Dominic Samra for providing the Python code used to generate the figures in this report and helping me throughout the project. Additionally, I would also like to thank my fellow summer students, David Lewis (who extracted the 1D profiles from the GCMs and ran all simulations for the F and K star models) and Georgina Hirst, for their collaboration on our wider project. I would like to thank Herbert Fruchtl, who gave me access to and assistance with the Kennedy computing cluster. Finally, I would like to thank Lord Laidlaw of Rothiemay and the Laidlaw Foundation for providing the funding for my research.

References

[1] X. Alexoudi, M. Mallonn, E. Keles, K. Poppenhäger, C. von Essen, and K. G. Strassmeier. Role of the impact parameter in exoplanet transmission spectroscopy. , 640:A134, Aug. 2020.

[2] R. Baeyens, L. Decin, L. Carone, O. Venot, M. Agúndez, and P. Mollière. Grid of pseudo-2D chemistry models for tidally locked exoplanets - I. The role of vertical and horizontal mixing. , 505(4):5603–5653, Aug. 2021.

[3] F. Debras, N. Mayne, I. Baraffe, E. Jaupart, P. Mourier, G. Laibe, T. Goffrey, and J. Thuburn. Acceleration of superrotation in simulated hot Jupiter atmospheres. , 633:A2, Jan. 2020.

[4] L. Delrez, A. Santerne, J.-M. Almenara, D. R. Anderson, A. Collier-Cameron, R. F. Díaz, M. Gillon, C. Hellier, E. Jehin, M. Lendl, P. F. L. Maxted, M. Neveu-VanMalle, F. Pepe, D. Pollacco, D. Queloz, D. Ségransan, B. Smalley, A. M. S. Smith, A. H. M. J. Triaud, S. Udry, V. Van Grootel, and R. G. West. WASP-121 b: a hot Jupiter close to tidal disruption transiting an active F star. *Monthly Notices of the Royal Astronomical Society*, 458(4):4025–4043, 03 2016.

[5] M. Gillon, D. R. Anderson, A. Collier-Cameron, L. Delrez, C. Hellier, E. Jehin, M. Lendl, P. F. L. Maxted, F. Pepe, D. Pollacco, D. Queloz, D. Ségransan, A. M. S. Smith, B. Smalley, J. Southworth, A. H. M. J. Triaud, S. Udry, V. Van Grootel, and R. G. West. WASP-103 b: a new planet at the edge of tidal disruption. , 562:L3, Feb. 2014.

[6] J. D. Hartman, D. Bayliss, R. Brahm, G. Á. Bakos, L. Mancini, A. Jordán, K. Penev, M. Rabus, G. Zhou, R. P. Butler, N. Espinoza, M. de Val-Borro, W. Bhatti, Z. Csubry, S. Ciceri, T. Henning, B. Schmidt, P. Arriagada, S. Shectman, J. Crane, I. Thompson, V. Suc, B. Csák, T. G. Tan, R. W. Noyes, J. Lázár, I. Papp, and P. Sári. HATS-6b: A Warm Saturn Transiting an Early M Dwarf Star, and a Set of Empirical Relations for Characterizing K and M Dwarf Planet Hosts. , 149(5):166, May 2015.

[7] C. Hellier, D. R. Anderson, A. Collier Cameron, M. Gillon, E. Jehin, M. Lendl, P. F. L. Maxted, F. Pepe, D. Pollacco, D. Queloz, D. Ségransan, B. Smalley, A. M. S. Smith,

J. Southworth, A. H. M. J. Triaud, S. Udry, and R. G. West. WASP-43b: the closest-orbiting hot Jupiter. , 535:L7, Nov 2011.

[8] C. Helling. Exoplanet Clouds. *Annual Review of Earth and Planetary Sciences*, 47:583–606, May 2019.

[9] C. Helling, N. Iro, L. Corrales, D. Samra, K. Ohno, M. K. Alam, M. Steinrueck, B. Lew, K. Molaverdikhani, R. J. MacDonald, O. Herbort, P. Woitke, and V. Parmentier. Understanding the atmospheric properties and chemical composition of the ultra-hot Jupiter HAT-P-7b. I. Cloud and chemistry mapping. , 631:A79, Nov. 2019.

[10] C. Helling, Y. Kawashima, V. Graham, D. Samra, K. L. Chubb, M. Min, L. B. F. M. Waters, and V. Parmentier. Mineral cloud and hydrocarbon haze particles in the atmosphere of the hot Jupiter JWST target WASP-43b. , 641:A178, Sept. 2020.

[11] C. Helling, D. Lewis, D. Samra, L. Carone, V. Graham, O. Herbort, K. L. Chubb, M. Min, R. Waters, V. Parmentier, and N. Mayne. Cloud property trends in hot and ultra-hot giant gas planets (WASP-43b, WASP-103b, WASP-121b, HAT-P-7b, and WASP-18b). , 649:A44, May 2021.

[12] C. Helling, P. B. Rimmer, I. M. Rodriguez-Barrera, K. Wood, G. B. Robertson, and C. R. Stark. Ionisation and discharge in cloud-forming atmospheres of brown dwarfs and extrasolar planets. *Plasma Physics and Controlled Fusion*, 58(7):074003, July 2016.

[13] C. Helling, M. Worters, D. Samra, K. Molaverdikhani, and N. Iro. Understanding the atmospheric properties and chemical composition of the ultra-hot Jupiter HAT-P-7b. III. Changing ionisation and the emergence of an ionosphere. , 648:A80, Apr. 2021.

[14] A. P. Showman and L. M. Polvani. Equatorial Superrotation on Tidally Locked Exoplanets. , 738(1):71, Sept. 2011.

[15] G. Torres, J. N. Winn, and M. J. Holman. Improved Parameters for Extrasolar Transiting Planets. , 677(2):1324–1342, Apr. 2008.

[16] V. Van Eylen, H. Kjeldsen, J. Christensen-Dalsgaard, and C. Aerts. Properties of extrasolar planets and their host stars: A case study of HAT-P-7. *Astronomische Nachrichten*, 333:1088, Dec. 2012.

[17] P. Woitke and C. Helling. Dust in brown dwarfs. III. Formation and structure of quasi-static cloud layers. , 414:335–350, Jan. 2004.